An experimental framework for determining wear in porous journal bearings operated in the mixed lubrication regime

S. J. Eder[a,*], C. Ielchici[a], S. Krenn[a], D. Brandtner[a]

[a] *AC2T research GmbH, Viktor-Kaplan-Straße 2, 2700 Wiener Neustadt, Austria*

Abstract

We present an experimental and analysis workflow to characterize the tribological behavior and the wear resistance of porous journal bearing systems operating at high loads and small rotational speeds. Our approach consists of a laser-instrumented tribometer that allows parallel testing of five bearings, an experimental procedure that is optimized for producing sufficient wear during mixed lubrication operation while maintaining realistic operating conditions, as well as several methods to visualize and quantify bearing wear. The simultaneous testing of five bearings prevents outliers from distorting the results and yields a statistical estimation of the performance variations between nominally equivalent tribosystems. We showcase our approach by analyzing the influence of the bearing material and its porosity on mixed-lubrication friction and wear.

Keywords: Porous bearing, Mixed lubrication, Wear measurement, Optical microscopy

Note: This is an author-created, un-copyedited version of an article published in *Tribology International*. Elsevier is not responsible for any errors or omissions in this version of the manuscript or any version derived from it. The Version of Record is available online at `https://doi.org/10.1016/j.triboint.2018.02.026`.

1. Introduction

Journal bearings are simple and cheap mass-production machine elements that operate together with a matching shaft of a drive. Porous Journal Bearings (PJBs) are produced from metal powders by sintering, and the resulting porous structure is impregnated with a lubricant like a sponge [1, 2]. The permanent oil circulation between the lubrication gap and the bearing's porous sliding face gives them the advantage of "life-time lubrication", i.e., they are maintenance-free for their entire service life of up to 10 000 hours [3, 4]. Due to this and their flexibility in design, they are very often used in industrial applications where an external supply of oil is not possible. PJBs are overwhelmingly operated in the hydrodynamic lubrication regime, so that the asperities of the bearing and the shaft never touch except during starting and stopping. However, there are several applications, e.g., in the automotive industry, such as power window lifts or windshield wipers, where mixed-lubrication conditions apply, i.e., operation at small rotational speeds and high loads[5, 6, 7]. Although the friction minimum is frequently located in this lubrication regime [8], the body and the counterbody constantly engage in direct contact, so the components are subjected to wear. This means that the requirements to the bearing material as well as the lubricant are quite different from those for hydrodynamic operation.

Much of the seminal work on PJBs was published between the 1950s and the 1980s [1, 2, 9]. However, there have been some very recent developments regarding the theory of PJB lubrication [10, 11] or the lack thereof [12], as well as the effect of laser surface texturing [13] or mesogenic fluids as novel high-performance lubricants [14] on friction and wear performance. The wear resistance of porous iron bearings additivated with boron nitride was also recently studied [15]. That said, it may be stated that literature dealing with PJBs operating in the mixed-lubrication and/or high-wear regime is scant.

Previous studies by some of the authors focusing on the hydrodynamic operation regime of PJBs [16] or on special phenomena such as cold-squealing [17] have been carried out on a dedicated porous bearing tribometer (SLPG). However, this device can only test one bearing at a time, and since wear tests usually run for several days, a simple but robust device was needed that can wear down several bearings in parallel, thus ensuring comparable operating conditions. An important benefit of this approach is that it allows us to quantify the variance in tribological performance and wear resistance that may result from fabrication tolerances or small inconsistencies in bearing impregnation or system assembly.

In this contribution, we will first give a detailed description of the custom-designed multiple bearing wear

*Corresponding author
Email address: `stefan.eder@ac2t.at` (S. J. Eder)

tribometer, with a special focus on the laser sensor instrumentation for reliable friction torque measurement at higher rotational speeds. We then discuss our experimental procedure that was optimized for the acquisition of statistically confirmed test results. Section 4 deals with three different approaches for visualizing and/or quantifying bearing wear. Finally, in Sect. 5, we present a short study to showcase the capabilities of our experimental and analysis framework that can be applied to rank various combinations of bearing material and lubricant according to their tribological properties and their wear resistance.

2. Multiple bearing wear tribometer (MSVT)

2.1. General features

To perform tribological experiments, a journal bearing test rig (MSVT) was developed and manufactured from scratch at AC2T research GmbH. The MSVT tribometer provides five independent test benches for parallel testing as shown in Fig. 1. These can be used for high-throughput parallel screening tests with different samples and/or parameter setups on one side, or for statistically confirmed testing with five nominally equal samples and parameter configurations on the other.

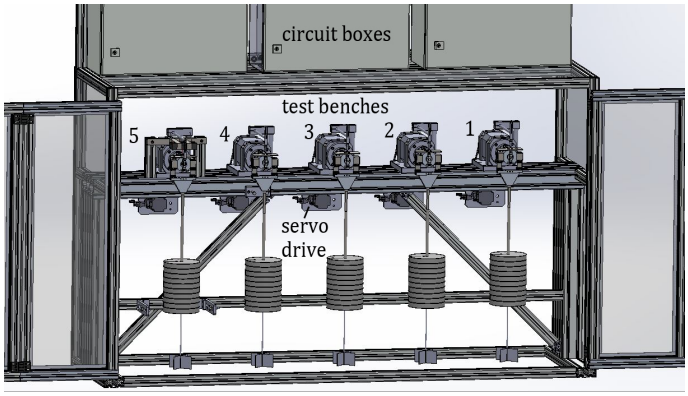

Figure 1: MSVT wear tribometer – Configuration of test benches.

Each test bench is controlled by an individual frequency converter that drives the associated servo motor. The relevant technical data of the motor is listed in Table 1. Each servo motor drives a high-precision spindle via a synchronous belt. At the spindle output, the test shaft is mounted through a jaw chuck. The journal bearing as a counterpart is mounted in a sample holder as shown in Fig. 2 (a).

Table 1: Technical data of servo motor.

Rated supply voltage	220 V, single phase
Nominal output power	200 W
Nominal speed	3000 min^{-1}
Torque: nominal/peak	0.64 / 1.92 Nm

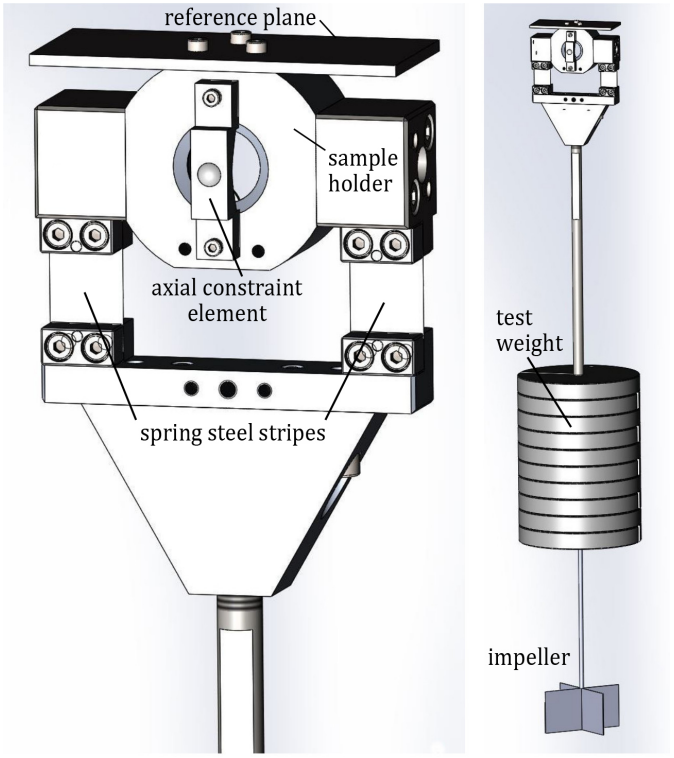

Figure 2: (a) Pendulum head with sample holder. (b) Total view of pendulum including weight and impeller.

To apply the test load, a rod with removable weights is connected to the sample holder through limp spring steel strips, which also avoids edge effects in the shaft-bearing-contact due to, e.g., asymmetric loading. Therefore, only the translation in axial direction is constrained to avoid axial sliding between bearing and shaft. The assembly shown in Fig. 2 (b) will be called pendulum henceforth. Below the weights, the pendulum rod is extended by an impeller that is dipped into a container filled with oil in order to damp undesired oscillations, see Fig. 3. During testing, the bearing temperature is measured continuously using a type K thermo-couple wire.

Two methods are applied to evaluate the friction torque, and hence the coefficient of friction. First, for drive control reasons the frequency converter continuously measures the electrical current that is used to power the servo motor. This electrical current is proportional to the resulting motor torque, which is thereby also calculated in the frequency converter and transferred to the measurement system through an adequate interface. By subtracting the running idle torque (including all the parasitic losses) from the measured signal, we can derive the remaining friction torque. This method does not yield the highest accuracy, but provides a suitable approximation of the tribological conditions during long-term testing at low rotational speeds. The second, more accurate, method measures the deflection of the pendulum from which the friction torque

can be derived. The laser instrumentation required for this approach is described in detail in the following Sect. 2.2.

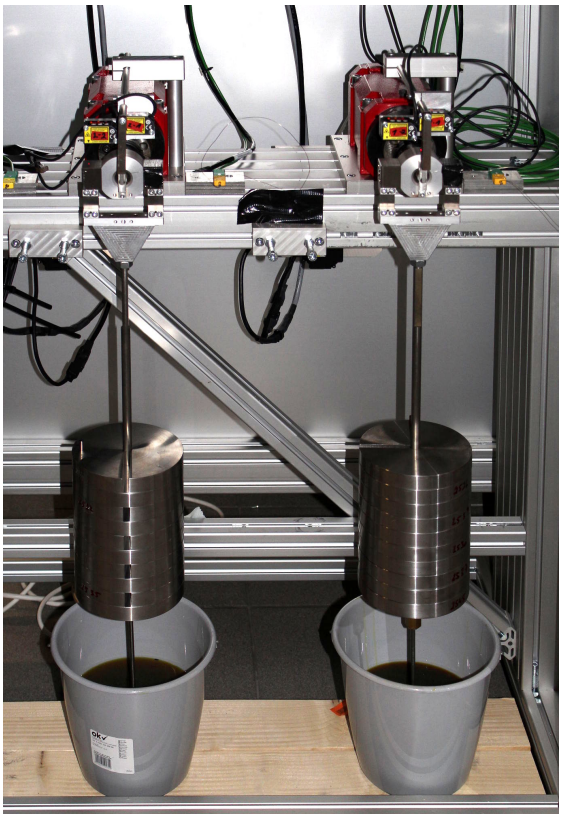

Figure 3: Two test benches of the MSVT tribometer in operation.

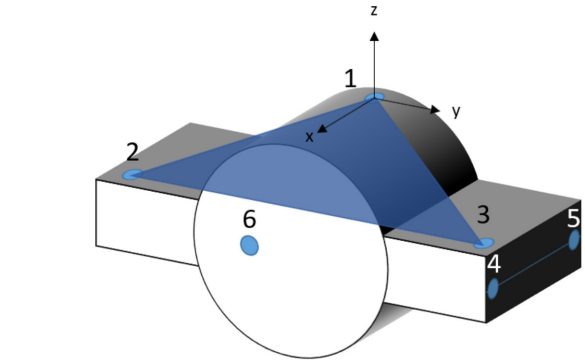

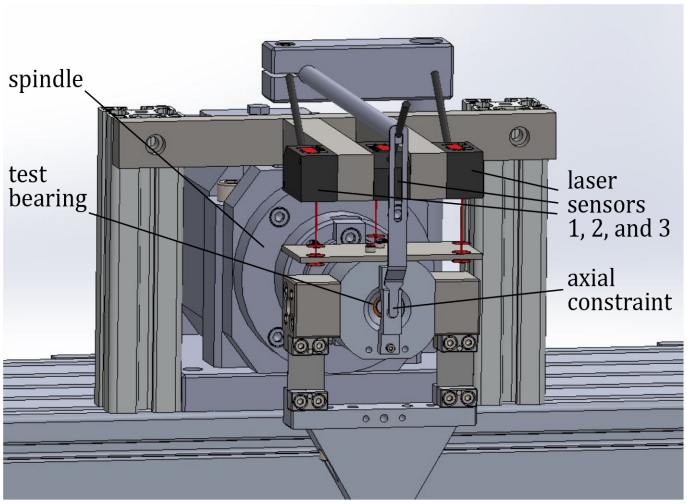

Figure 4: (Top) Schematic distribution of six laser spots for determining all degrees of freedom. (Bottom) Sensor placement above the pendulum head after reduction to three spots.

2.2. Laser sensor instrumentation

The laser measuring system is mounted above each pendulum head on the MSVT. The system consists of six sensors, which are arranged in the three-dimensional space and measure the position of the pendulum head of an MSVT test bench, see Fig. 4 (top) for a schematic arrangement of the laser spots in the reference coordinate system. Three of the sensors mounted above the pendulum on a plane parallel to the xy-plane, measuring changes in the vertical distance (z-direction). Two more are aligned parallel to the x-direction at a constant distance in the y-direction and measure the lateral displacement of the pendulum. The last sensor points towards the front of the pendulum and measures position changes of the pendulum head along the x-direction. The used sensors are laser triangulation sensors providing an analog voltage output from 0 V to 5 V. This output corresponds to a measuring range of 10 mm and has a resolution of 6.46 μm. The mounting of the sensors was designed so that the installation of samples can be carried out as unhindered as possible.

In order to describe the rigid body displacement of the pendulum in space, it is necessary to apply a rotation matrix in three dimensions. To be more specific, this

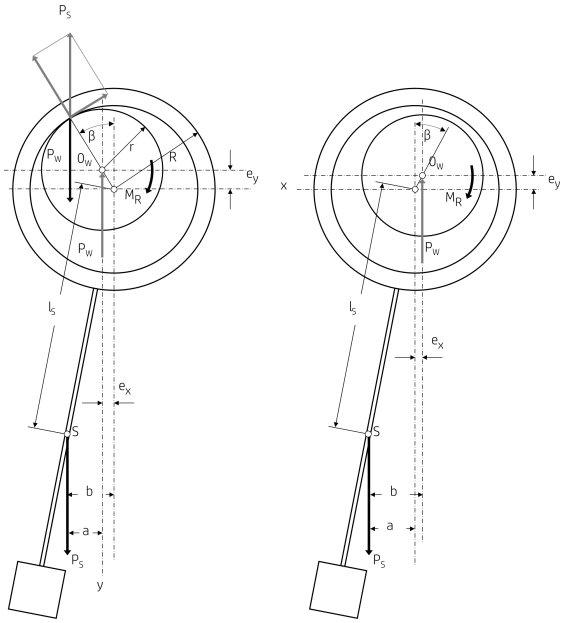

Figure 5: Forces in the pendulum and comparison between dry or mixed-lubricated (left) and fully lubricated state (right) [19, 20].

rotation matrix can be decomposed into three basic rotations around α, β, and γ. Each basic rotation describes a rotation about one axis of the Cartesian coordinate system [21]. Together with the translations u_x, u_y, u_z, the following equation can be found:

$$\overrightarrow{R_i}(t) = \overrightarrow{R_0}(t) + \overrightarrow{U}(t) + X(\alpha(t), \beta(t), \gamma(t)) \cdot \left(\overrightarrow{R_i}(0) - \overrightarrow{R_0}(0) \right) , \tag{1}$$

with

$$\overrightarrow{U}(t) = \begin{pmatrix} u_x \\ u_y \\ u_z \end{pmatrix} ; \quad i = 1, .., 6; \quad \overrightarrow{R_0} = \begin{pmatrix} 0 \\ 0 \\ 0 \end{pmatrix} \forall t \ . \tag{2}$$

It should also be mentioned that i is the number of sensors, which also represents the number of degrees of freedom. R_0 is the center of the coordinate system and R_i represents the coordinates of each sensor. Now, the time development of all degrees of freedom can be determined using a program routine. For the friction torque, above all the pendulum displacement α is decisive. By taking a closer look at the equation, it can be argued that only two sensors would be enough to determine α. However, since mounting these sensors perfectly aligned with the coordinate system is non-trivial, the accuracy can be greatly improved by installing sensor number three, thus spanning a plane in space. Considering this, the matrix is reduced to

$$\begin{pmatrix} \Delta z_1 \\ \Delta z_2 \\ \Delta z_3 \end{pmatrix} = \begin{pmatrix} 1 & y_1(0) & -x_1(0) \\ 1 & y_2(0) & -x_2(0) \\ 1 & y_3(0) & -x_3(0) \end{pmatrix} \begin{pmatrix} u_z \\ \alpha \\ \beta \end{pmatrix} \ , \tag{3}$$

in matrix notation

$$\underline{\Delta X} = \underline{K} \ \underline{U} \ . \tag{4}$$

$\underline{U}$ now consists of the translation in z-direction and the displacements α and β, which are different from the ones in Eq. (1), and provides the parameters required for the determination of the friction torque. Due to the reduction of the number of sensors, the mounting is reduced to a more handy construction as shown in the bottom panel of Fig. 4, but also the calculation time of the routine and the amount of data is minimized and no longer includes unnecessary information.

A similar approach of friction and position measurement was used in some recent work of Trachsel *et al.* [18]. There, only two degrees of freedom were measured using high precision laser sensors to evaluate the two vectorial components of the radial eccentricity. The investigations performed in [18] focused on small journal bearings with smaller clearance under loadings up to approximately 0.1 MPa, which is less by a factor of 30 than in the case study discussed below. Furthermore, in [18] the test load is applied in a different way (without pendulum), therefore the measured friction torque is corrected by additional displacement measurement.

It must be ensured that when determining the torque of a sliding bearing, a distinction must be made between a dry-running bearing and a lubricated one, see Fig. 5. While running dry or under mixed lubrication, as depicted on the left side of Fig. 5, the internal contact forces between shaft and bearing P_W have to be in equilibrium with the external load P_S. Compared to the direction of rotation of the shaft, its displacement inside the bearing is reversed. Under hydrodynamic conditions, as depicted in the right panel of Fig. 5, the shaft displacement follows the direction of the rotation because of the hydrodynamic fluid pressure in the diverging gap. Furthermore, the point from which the measurement of the pendulum displacement is made has to be specified. The influence of relocation torque is eliminated by placing the measuring line pointing in the y-direction into the fixed center of the shaft. This reduces the equation for determining the friction torque of the pendulum to

$$M_R = P_S \cdot a \ , \tag{5}$$

which is the product of the pendulum load and the displacement from the origin [19, 20].

3. Experimental workflow

The porous journal test bearings were custom fitted by the bearing manufacturer to have a bore diameter of 8.033±0.001 mm, leading to an average diametric gap of 28 μm or 0.35% to the hardened and tempered steel shaft with a surface hardness ranging from HRA 78 to HRA 84. The above-average clearance is intended to make the contact less conformal and should lead to higher wear. The bearings are shipped impregnated only with the oil used for calibrating the bore hole, so they arrive with an oil filling of approximately 5%.

A 0.6 mm diameter hole for the thermocouple is drilled into the planar front face of the bearing, close to the bearing surface, and then the sample is engraved with a unique bearing ID. The hole also doubles as a marker for the 12 o'clock position of the bearing to ensure consistent assembly and orientation. The bearing is cleaned by boiling it in toluene under reflux and leaving it in an evacuated desiccator over night. It is then impregnated with the desired porous bearing lubricant using a desiccator and a drying oven.

In the above workflow, the desiccator pressure always lies above vapor pressure of the respective oil so that no lubricant components evaporate. Finally, based on the empty and impregnated bearing weights as well as the bulk densities of the bearing material and the oil, it is ascertained that all bearings are filled to at least 95%.

As the test bearings have a projected bearing surface of 8 mm × 10.5 mm = 84 mm^2, a load of 25 kg corresponds to a mean pressure of 2.92 MPa, which lies at the upper end of the load range experienced by porous journal bearings in real operation.

We first performed preliminary tests on the MSVT, designed to determine the long-term rotational speed profile

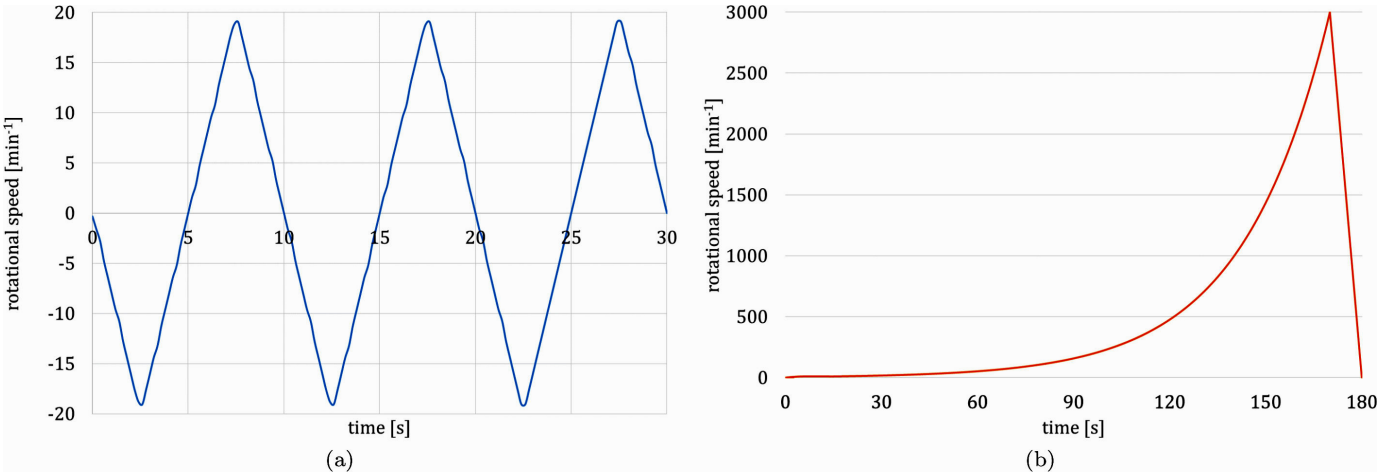

Figure 6: Rotational speed profiles: (a) Bidirectional saw-tooth profile with $\omega = \pm 20$ min^{-1} for mixed lubrication operation. (b) Logarithmic Stribeck ramp profile.

that produces the highest amount of wear in the shortest time. We tested at five maximum rotational speeds ω_{max}, which took values of 750, 300, 150, 50, and 20 min^{-1}. These maximum rotational speeds translated into three types of profiles:

- ω_{max} constant
- unidirectional saw-tooth profile: $0 \rightarrow \omega_{max} \rightarrow 0$
- bidirectional saw-tooth profile: $-\omega_{max} \rightarrow \omega_{max}$

In the initial trials, these profiles were preceded by a 6 h running-in period at 1000 min^{-1}, but this was soon given up, as hardly any additional wear occurred in these run-in systems, regardless of the rotational speed profile. The preliminary tests clearly showed that the bidirectional saw-tooth profile with $\omega_{max} = 20$ min^{-1}, see Fig. 6 (a), produced the highest amount of wear, and that it was sufficient to run this mixed-lubrication program for 44 h. Note that the unidirectional saw-tooth profile gave the same qualitative results as the bidirectional one, only less pronounced. The chosen profile reflects systems that are repeatedly switched on and off or operated from the resting position (power window lifts, windshield wipers, throttle valves, etc.). During the test period, the estimated coefficient of friction (CoF), calculated from the torque of the drive, is recorded. To simplify the resulting signal, which naturally features overall noise and especially spikes at rotational speeds close to zero, only the values at $\omega = \pm 20$ min^{-1} are plotted over time. This leads to two curves, one for clockwise rotation and one for counterclockwise rotation. The general trend of this mixed-lubrication CoF may be used as a diagnostic instrument for illustrating the running-in of the system or revealing anomalies or catastrophic events during operation. Some examples of such curves are discussed in Sect. 5.

As an additional means of tracking the running-in of the system, four consecutive Stribeck curves [22] are recorded after 1, 2, 3, 4, 5, 8, 11, 14, 17, 20, 28, 36, and 44 h of mixed lubrication operation, which adds an extra 2.5 h of duration to the entire test procedure. The associated rotational speed profile shown in Fig. 6 (b) for one such curve was designed using a logarithmic time axis for three reasons: (1) to keep the application of frictional energy into the system to a minimum and thus keep the temperature low, (2) to allow the pendula sufficient time to recover from their initial oscillations resulting from breaking loose from the static friction regime, and (3) to maximize the data resolution around the low rotational speeds up to approximately 300 min^{-1}, where the minimal CoF, i.e., the onset of hydrodynamic lubrication, is assumed. The four associated curves are then averaged, and the resulting thirteen "master curves" are plotted together in a rainbow-style coloring scheme so that the dark blue curve represents the Stribeck curve after 1 h of mixed lubrication operation, and the dark red one illustrates the behavior after 44 h. If the system runs in smoothly, the CoF minimum will continuously decrease over time, see the examples in Sect. 5.

4. Wear measurement and imaging

4.1. Schwenk OSIMESS

The Schwenk OSIMESS is a tactile two-point comparison instrument intended for manually measuring the inner diameters of bore holes ranging from 1 mm to 40 mm [23]. It consists of a measuring stand, a dial gauge indicating unit, a retractable holder, a needle serving as an actuating wedge, and a set of split-ball probes of various diameters with matching reference setting rings. This purely mechanical device is suitable for obtaining a fast, cheap, quantitative measurement of the bearing diameter change due to wear [24]. After insertion of the probe into the bearing, the former is split open by the precision-ground wedge of the needle, bringing the two halves of the probe into contact with the inner bore surface. The resulting radial movements of the split probe are transferred to the

indicating unit backlash-free. Simple as the method may be, it can achieve a repeatability of <1 μm in radial direction, with a measuring range from 7.7 mm to 8.3 mm when using the 8 mm probe. Dozens of bearings can be measured per hour in this fashion.

Before measuring the worn bearing diameters, all bearings are freed of residual oil and debris by pulling a soft, lint-free cloth through the bearing bore. All diameter measurements were performed at the front and the rear ends of the bearing (approximately 0.5 mm away from the bearing edges) as well as in the bearing center. Note that although the bearings are always originally aligned before the measurement according to the position of the 12 o'clock hole for the thermocouple, the maximum diameter of the bore hole is found by rotating the bearing. Therefore this method is not well suited for obtaining the azimuthal position of the greatest diametric change.

4.2. Micro-Epsilon boreCONTROL

For the qualitative, non-destructive inspection of the worn bearing surfaces [25], we used a customized bore hole imaging system, named boreCONTROL, by Micro-Epsilon [26]. The measurement system consists of a sensor with an integrated rotary drive, a motor controller, a sensor controller, and an exchangeable sensor lance. boreCONTROL is based on confocal chromatic sensor technology and allows surface inspection using intensity measurement. The rotating sensor lance produces circular measurements, and the system provides non-contact diameter measurements in bore holes and cavities, see Fig. 7. It features short measurement cycles due to its high sampling rate, fair repeatability and accuracy, as well as optical temperature compensation.

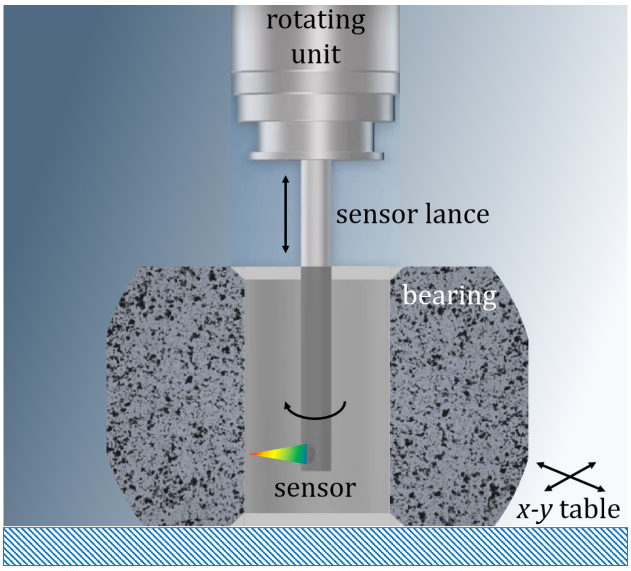

Figure 7: Side view sketch of the boreCONTROL system measuring the inside of a porous bearing (not to scale).

For the 8 mm bore holes in this work, we used the sensor lance for the 4–10 mm measuring range. The diameter of the measuring spot, which effectively limits the lateral resolution, is approximately 40 μm. The repeatability in radial direction is ± 1 μm, and the radial linearity is ± 5 μm. The measuring rate can be varied between 0.1 and 25 kHz. For each measurement, three parameters must be set to obtain a good image of the bearing: the scan rate in kHz, the shutter time in μs, and the rotation speed in Hz. Generally there are two different types of surface to deal with. For shiny and smooth surfaces, it is possible to use fast acquisition parameters with a 10 kHz scan rate and approximately 50 μs shutter time. Rough and very dark surfaces require a lower scan rate, e.g., 5 kHz, and a longer shutter time like 200 μs to compensate the higher light absorption. Two different settings are used to generate hybrid images of bearings whose cylinder barrels feature a wide range of reflectivities. The bearings are measured by aligning it according to the 12 o'clock position of the bore hole using the x-y table and the polar diagram. After a preliminary scan, the acquisition parameters may require some fine-tuning before the accurate measurement can begin. The raw data are recorded to an ASCII file. With this method it is possible to measure between 4 and 5 bearings per hour. All bearings are measured with a scan configuration of 1050 sensor rotations, covering the bearing length of 10.5 mm.

One challenge lies in correcting tiny misalignments between the z-axis of the sample and that of the laboratory system. This is more difficult than it may seem, as the porous structure of the unworn bearing surface provides a noisy data basis for the fitting to an ideal cylinder, compounded by a speckling effect that leads to large artificial differences between two neighboring image points. Furthermore, a heavily worn bearing may lead to complete failure of an automatized fitting procedure, as the worn surface is usually much smoother than the unworn one, and the cross-section of such a bearing more resembles an ellipse than a circle. The most stable approach to aligning the z-axis of the bearings was based on the iterative closest point (ICP) algorithm [27, 28].

Summarizing, it can be stated that the boreCONTROL device is well-suited for producing complete 360° images of the worn bearing surfaces, giving a good idea of the position, size, and quality of the wear scar, cf. the images at the end of Sect. 5. However, since the unworn porous surfaces are very noisy and the alignment of the z axis is non-trivial, a quantitative evaluation of a wear volume is not possible with this approach.

4.3. Alicona InfiniteFocus G5

The Alicona InfiniteFocus G5 is a 3D micro coordinate measurement machine and surface roughness measurement device in one system. Depending on the objective lens magnification, the Alicona delivers lateral resolutions between 0.44 μm and 3.5 μm and vertical resolutions ranging from 10 nm to 410 nm. Topographic measurement by focus variation is performed by determining the best focus position of the optical sensor elements. The focus position

is related to a certain distance between the objective lens and the sample, therefore the sample is vertically scanned at different distances or focus positions. The best focus position is calculated by determining the contrast between each pixel and its respective neighbors in the CCD array. In addition to the topography, the system simultaneously provides the true color image of the sample. This technique allows surveys of machine parts and components regarding wear and geometrical changes within reasonable measuring times.

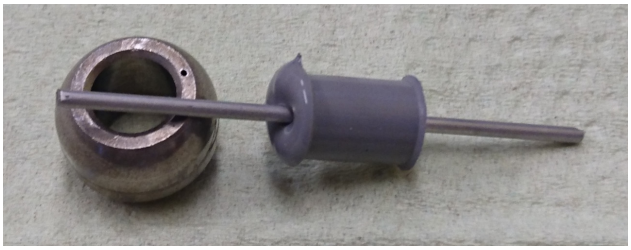

Figure 8: Worn porous bearing and silicone replica of its inner bearing surface. Note the 0.6 mm hole for the thermo-couple in the front face of the bearing.

The main application of the Alicona InfiniteFocus G5 in this work is the fast imaging and topographical analysis of worn shafts, which can be measured directly due to their convexity. It was also used as an alternative to the boreCONTROL device for measurements of the worn bearing surface topography. Because of the closed concave surface geometry of the bearing, this inner cylinder surface is not fully visible, so an appropriate casting material is used to create a replica of the inner bearing surface. We used a two-component, gray-colored silicone mold, which hardens within several minutes, after which the settled replica can be extracted and measured. In order to better manipulate the resulting silicone cylinder, a shaft is placed in the middle of the molds. This makes it possible to measure the entire silicone cylinder surface while rotating the sample and stitching the results to a final 3D image using the Alicona Measurement Tools software. Even without rotation, the reflectivity of the silicone mold allows simultaneous imaging of approximately 120° of the bearing surface, which is sufficient for most wear scars.

Figure 9: Real 3D-images of an exemplary worn bearing (left) and matching shaft (right) surface measured with the Alicona 3D-microscope.

Figure 8 shows a typical replica ready for topography measurement with the Alicona. In a first measurement step, realistic images of the contacting bearing and shaft surfaces are acquired, see Fig. 9. In a following post-processing data operation, the shape of the original cylinder can be removed from the measurement data of the worn bearing. From the resulting color plots, as shown in Fig. 10, the wear depth can be estimated. In Fig. 10 (a) the blue-colored area near the middle of the bearing's sliding face represents "negative wear height" in the range of –5 μm to –10 μm, which results from material build-up due to the agglomeration of wear debris. The green and red-colored areas exhibit regular wear in the shape of grinding marks caused by abrasives.

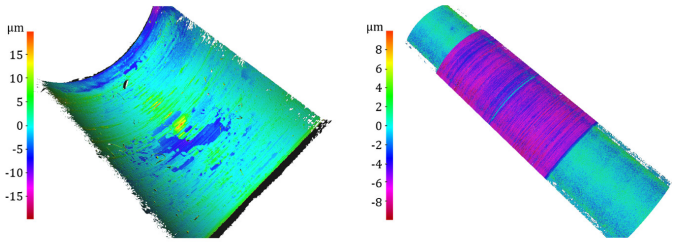

(a) (b)

Figure 10: Color plots illustrating wear on the bearing (a) and shaft surfaces (b).

During some casting procedures it was observed that the hardened replica can have strong adhesion to the journal bearing. In such cases it could be difficult to separate the replica from the bearing so that high forces and deformations have to be applied during extraction. This can lead to residual deformations on the replica. Under such circumstances, the topography measurement can only be used for a qualitative surface characterization. The worn shaft in Fig. 10 (b) shows a mostly uniform wear depth of approximately 6 μm in addition to distinct scratch marks in circumferential direction. In the middle of the wear track there is a narrow region with a smaller wear depth, which can also be observed in the plotted 2D wear profile shown in Fig. 11.

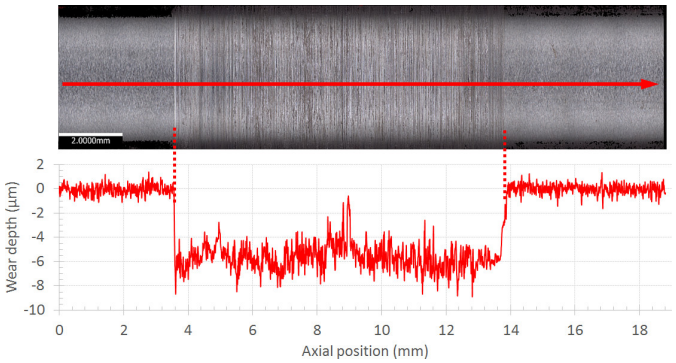

Figure 11: Wear profile on shaft in axial direction.

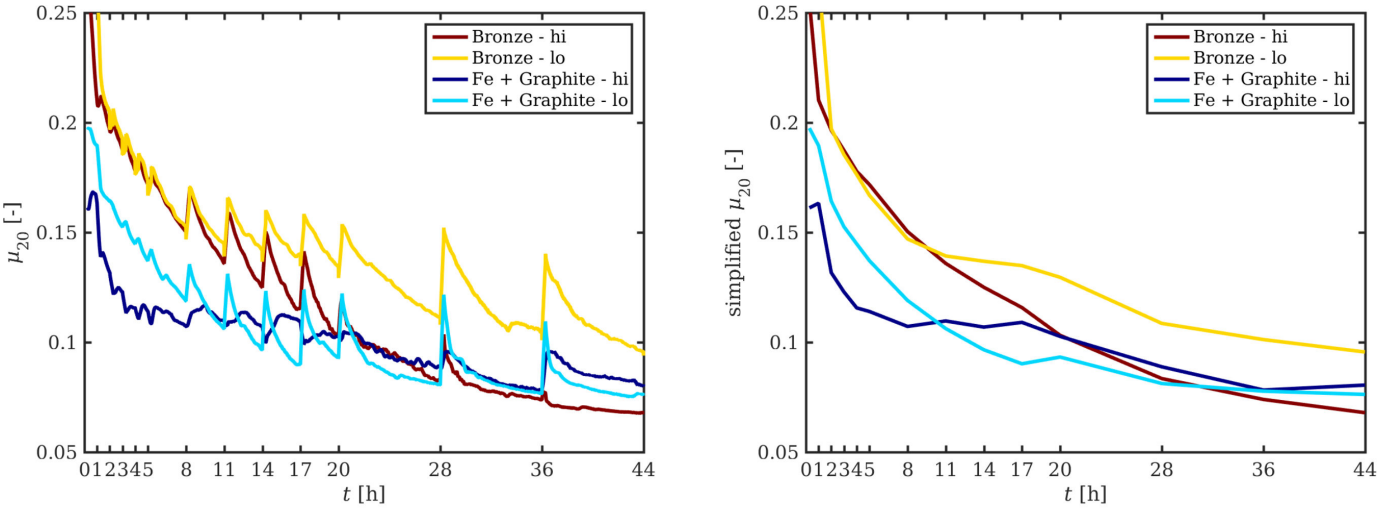

Figure 12: Time evolution of the CoF in the mixed lubrication regime at 20 min^{-1}. (a) Full resolution including CoF spikes due to heating up during Stribeck ramps. (b) Simplified version showing only values immediately before Stribeck ramps.

When applied to bearing surface imaging, this method is time-consuming (approximately 1 hour for one sample) because of the elaborate replica sample preparation, and it has limited reproducibility due to uncontrollable plastic deformation suffered by the silicone molds when being extracted from the bearings.

5. Case study

In this section we will showcase what the MSVT tribometer is capable of in conjunction with its laser instrumentation, the OSIMESS wear measurement, and the boreCONTROL imaging of the worn bearing surfaces. The chosen example constitutes a small portion of a much larger study consisting of more than 140 bearing–lubricant combinations that were tested for their tribological performance and their wear resistance. In this study, which will be analyzed and discussed in a forthcoming publication, all combinations were first tested only once for a pre-screening of general trends, after which the most promising combinations as well as implausible results were checked in batches of 5 nominally identical bearing–lubricant combinations for statistical confirmation. This allows a relatively safe distinction between typical behavior and statistical outliers.

The lubricant used for all the bearings in this exemplary case study is an ester oil with a base oil viscosity of 68 mm^2/s at 40 °C and a lithium thickener. As bearing materials, we used pure sinter bronze bearings and sinter steel bearings with 3wt% of Cu and 1.5wt% of graphite as a solid lubricant. Both materials were tested in a high-density ("hi") and a low-density ("lo") version. The mean porosities were 19.1% and 23.5% for the bronze bearings, respectively, and 18.5% and 23.4% for the steel bearings.

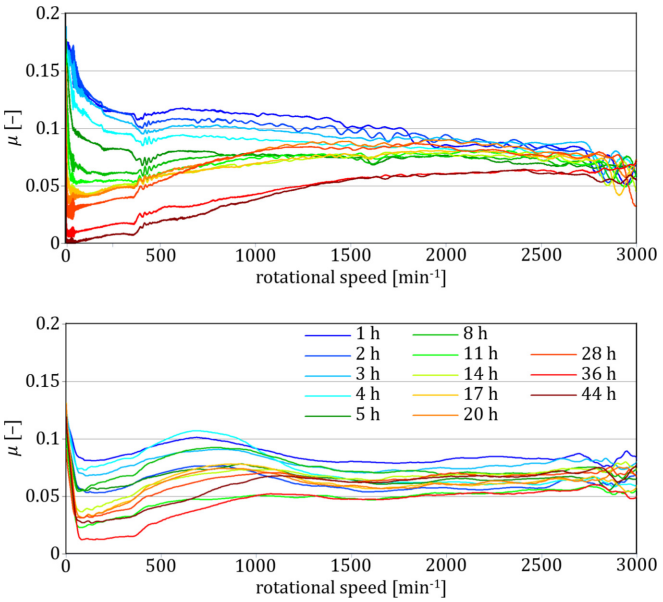

Figure 13: Monitoring the running-in process of two porous journal bearing systems using Stribeck curves recorded after the time intervals indicated by the respective color in the legend. The shown curves are averaged over four consecutive rotational speed ramps. Error ranges are not shown to improve clarity. Top: Bronze - hi. Bottom: Fe + Graphite - hi.

5.1. Friction

As described in Sect. 3, the friction torque is measured via the drive torque of the individual test benches, so that the CoF at 20 min^{-1}, μ_{20}, can be monitored over time. The resulting curves, shown in Fig. 12, are then used as a diagnostic device to assess if the system is running in properly and converging to steady-state operation, or if larger-scale wear events lead to intermittent increases of μ_{20}. Mixed-lubrication operation is interrupted at the in-

tervals mentioned above (and marked on the abscissa in Fig. 12) for the recording of Stribeck curves whose data has been removed from the respective graphs, μ_{20} exhibits discontinuities at these points in time, see Fig. 12 (a). For a simplified view of the data, focusing on the running-in, only those μ_{20} values recorded immediately before the Stribeck ramps can be plotted over time, see Fig. 12 (b).

By recording Stribeck curves at 13 points in time during the mixed-lubrication regime testing, it was possible to monitor the formation of a hydrodynamic regime as well as the migration of the friction minimum to smaller CoF values and rotational speeds, see Fig. 13 for two examples. Here, the rainbow-style coloring scheme goes from blue (towards the beginning of the test) to dark red (end of the test after 44 h). The lowering of the friction minimum over time is obvious for both shown examples, and the formation of a stable hydrodynamic branch of the Stribeck curve is more pronounced for the bronze bearing. The oscillations/kinks in the curves at the rotational speed of approximately 400 min^{-1} are likely due to a resonance phenomenon in the MSVT tribometer.

5.2. Wear

Before discussing the wear results, it should be noted that the porous bearing lubricant used in this example case has generally proven to maintain high wear resistance paired with a wide range of bearing materials. The obtained bore diameter changes due to wear are therefore in the single-digit micron range, which according to the bearing manufacturer may be considered mere contact conformization and not as wear *per se*. For comparison, a combination of a low-density pure sinter steel bearing paired with a silicone oil led to diameter differences of up to 200 μm using the same testing procedure. The column charts shown in Fig. 14 were obtained by measuring the diameters of the worn bearings near the front, center, and rear, using the OSIMESS method, and averaging over all 5 bearings run in parallel. One outlying dataset was removed from the results for Bronze - lo, which would have pushed the average values to 5–10 μm and considerably lengthened the error bars. It can be considered statistically confirmed that the bearings wear down more around the edges than in the center, which will be corroborated by the bearing surface images presented later on. The higher wear obtained for the low-density Fe + Graphite bearing compared with the higher-density variant is actually a trend that is maintained throughout the larger part of the pre-screening tests, so that it can be assumed that bearing porosity has an important influence on wear resistance in mixed-lubrication operation.

As the boreCONTROL device was only available for two weeks shortly after the pre-screening tests had been completed, the worn bearing surfaces shown in Fig. 15 are not a subset of the ones whose wear data led to the column charts in Fig. 14. However, the results obtained in the pre-screening tests fit in well with those conducted

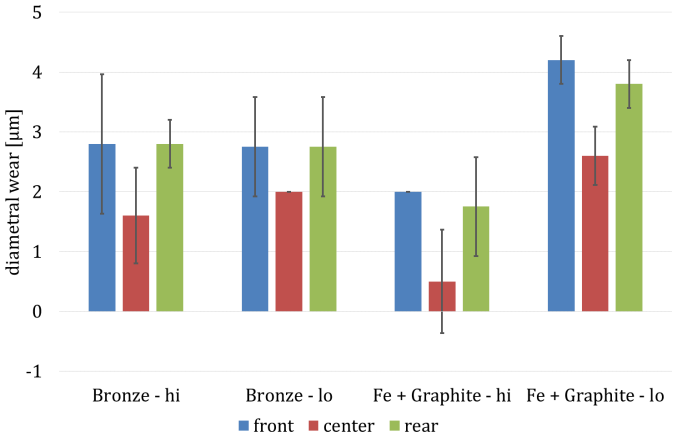

Figure 14: Diametric wear at the front, center, and rear of the bearings, averaged over 5 bearings operated in parallel. One outlying dataset was removed from the results for Bronze - lo.

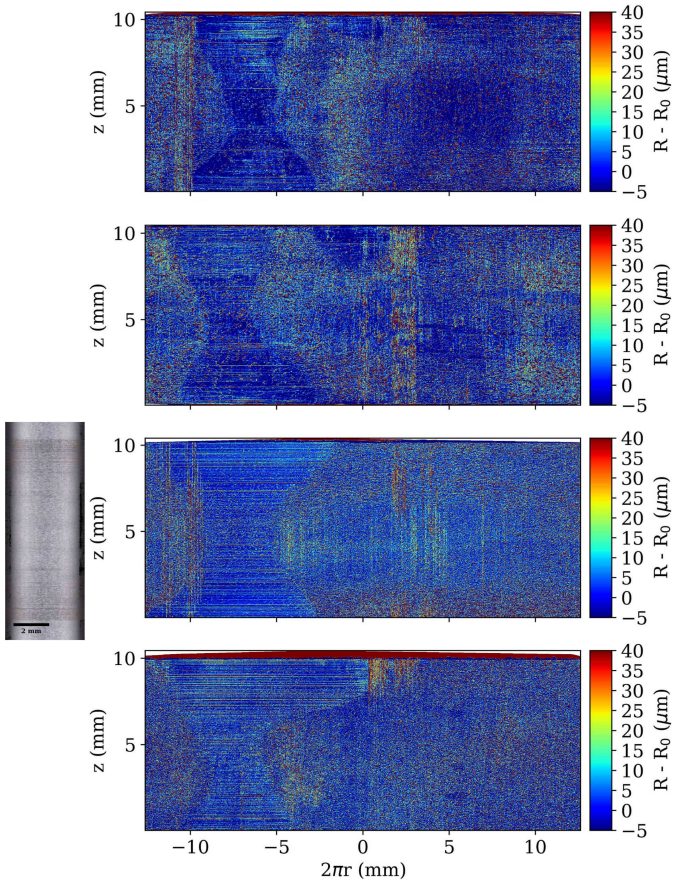

Figure 15: z-axis-aligned boreCONTROL bearing surface maps of the four bearing types, acquired during pre-screening tests. From top to bottom: Bronze - hi, Bronze - lo, Fe + Graphite - hi, Fe + Graphite - lo. Wear marks can be seen in the left half of the maps, whereas the right half is dominated by the unworn porous structure. The "front" of the bearings (as referenced in Fig. 14) is at the $z = 10$ mm position. The third map is complemented by an exemplary Alicona image of the corresponding shaft.

in parallel, so that the visualizations of the worn bearing surfaces can be considered representative. What can be seen immediately in the images is that the extreme

values of the coloring scheme, representing the deviation from the ideal cylindrical bore hole, occur mainly in the unworn, porous portion of the bearing surface, as well as in scratches orthogonal to the running direction that result from removing the bearing from the shaft. Although the wear marks themselves are only in the single-digit micron range and would therefore only have little contrast with the original bearing diameter shown in blue, the border between worn and unworn surface is clearly visible in all four shown examples, revealing an hourglass-shaped wear scar in all cases. The presented imaging technique would also immediately reveal the occurrence of edge-runners, which would be characterized by predominantly point-symmetrical wear marks, e.g., a parabolic scar in the top left and another inverted one at the bottom right. Due to the self-adjusting construction of the MSVT tribometer, we hardly ever observed such edge-runners. The third bearing surface visualization from the top in Fig. 15 is complemented by an exemplary Alicona image of the corresponding shaft. Note that several circumferential wear marks can be found at identical axial positions on the bearing surface and the shaft, whereas in general there is an even wear pattern over the entire contact area.

6. Summary and Conclusion

We have discussed an experimental and analysis workflow designed for studying and ranking the tribological performance and wear resistance of highly loaded and slow-running porous journal bearings. A custom-designed bearing tribometer allows either high-throughput screening tests or parallel testing of equivalent sample pairings and testing parameters for statistically confirmed results. The rotational speed profile was optimized towards mixed-lubrication operation and maximum bearing wear within a 46.5 h testing routine, so that up to 15 samples can be tested per week. We presented several methods to measure and visualize bearing wear, and our brief case study shows how all elements are applied in practice. In an upcoming publication, we will describe a large-scale study including more than 140 different pairings of bearing material and lubricant, making use of the devices and methods laid out in this work. There, it will be shown how the preliminary screening tests form the basis for a proper design of experiments, and how the following detailed parallel-testing leads to statistically confirmed results that can be translated into rankings of bearing–oil combinations according to various tribological properties.

Acknowledgment

This work was funded by the Austrian COMET-Program (Project K2, XTribology, no. 849109) and carried out at the "Excellence Centre of Tribology". The authors would like to thank Micro-Epsilon (Ortenburg) for providing them with their mobile, non-commercial boreCONTROL measuring device for two weeks. Thanks to Stefan Mayerhofer and Rainer Jahn for constructing and building the MSVT tribometer, Reinhard Grundtner for programming the software, Christoph Haslehner and Bettina Ronai for carrying out the experimental work, Marilu Miranda-Medina for assisting with the boreCONTROL imaging, Tetyana Khmelevska for measuring the shaft topographies, Pedro O. Bedolla for implementing the ICP algorithm, and to Tobias Binder for image post-processing. We would also like to thank Friedrich Franek for lively discussions about the manuscript and for making many useful suggestions.

References

[1] V. Morgan, A. Cameron, Mechanism of lubrication in porous metal bearings, Proceeding conference on Lubrication and Wear (1957) 151–175.

[2] A. Braun, Porous bearings, Tribology International 15 (5) (1982) 235–242.

[3] N. Veloff, A. Nadkarni, T. Murphy, Better performance for self-lubricating bronze bearings, Metal Powder Report 61 (8) (2006) 31–41.

[4] E. Durak, Experimental investigation of porous bearings under different lubricant and lubricating conditions, KSME International Journal 17 (9) (2003) 1276–1286.

[5] Q. J. Wang, F. Shi, S. C. Lee, A mixed-lubrication study of journal bearing conformal contacts, Journal of Tribology 119 (3) (1997) 456–461.

[6] F. Shi, Q. J. Wang, A mixed-TEHD model for journal-bearing conformal contacts—part I: model formulation and approximation of heat transfer considering asperity contact, Journal of Tribology 120 (2) (1998) 198–205.

[7] Q. J. Wang, F. Shi, S. C. Lee, A mixed-TEHD model for journal-bearing conformal contact—part II: contact, film thickness, and performance analyses, Journal of Tribology 120 (2) (1998) 206–213.

[8] H. Spikes, Mixed lubrication—an overview, Lubrication Science 9 (3) (1997) 221–253.

[9] R. Raman, L. V. Babu, Tests on sintered bearings with reduced oil contents, Wear 95 (3) (1984) 263–269.

[10] M. Trachsel, R. Pittini, J. Dual, A combined approach to study and model the effect of viscous heating in small porous, self lubricating journal bearings, Tribology International 116 (2017) 199–207.

[11] A. Sakim, M. Nabhani, M. El Khlifi, Non-newtonian effects on porous elastic journal bearings, Tribology International 120 (2018) 23–33.

[12] T. D. Shinde, P. Gajjal, Tribological behaviour for friction of composite dry journal bearing, International Journal of Engineering Technology Science and Research 4 (8) (2017) 1032–1037.

[13] N. Sharma, S. Kango, R. K. Sharma, Sunil, Investigations on the effects of surface texture on the performance of a porous journal bearing operating with couple stress fluids, International Journal of Surface Science and Engineering 8 (4) (2014) 392–407.

[14] T. Amann, A. Kailer, S. Beyer-Faiß, W. Stehr, B. Metzger, Development of sintered bearings with minimal friction losses and maximum life time using infiltrated liquid crystalline lubricants, Tribology International 98 (2016) 282–291.

[15] W. Urbaniak, T. Kaldonski, T. Kaldonski, Z. Pawlak, Hexagonal boron nitride as a component of the iron porous bearing: friction on the porous sinters up to 150° C, Meccanica 51 (5) (2016) 1157–1165.

[16] I. A. Neacşu, B. Scheichl, G. Vorlaufer, S. J. Eder, F. Franek, L. Ramonat, Experimental validation of the simulated steady-state behavior of porous journal bearings, Journal of Tribology 138 (3) (2016) 031703.

[17] S. J. Eder, D. Bianchi, I. A. Neacşu, G. Vorlaufer, An experimental and signal analysis workflow for detecting cold-induced noise emissions (cold squealing) from porous journal bearings, Mechanical Systems and Signal Processing (under review).
[18] M. Trachsel, R. Pittini, J. Dual, Friction and 2D position measurements in small journal bearings, Tribology International 102 (2016) 555–560.
[19] H. Detter, K. Holecek, Der Reibwiderstand und die Beanspruchung von feinmechanischen Lagern im Trockenlauf bei kleinen Gleitgeschwindigkeiten, Feinwerktechnik 74 (1970) 11.
[20] H. Detter, A study of the operating behavior of precision pivot bearings, Wear 26 (1) (1973) 121–132.
[21] M. Meywerk, CAE-Methoden in der Fahrzeugtechnik, Springer, 2007.
[22] X. Lu, M. Khonsari, E. Gelinck, The stribeck curve: experimental results and theoretical prediction, Journal of Tribology 128 (4) (2006) 789–794.
[23] http://www.schwenk-lmt.de/sidebar/download_2_ENG/24/Osimess_en_2010.pdf; [accessed 15 February 2018].
[24] P. Bauer, Grundlagen und Geräte der technischen Bohrungsmessung, Vol. 17, Springer-Verlag, 2013.
[25] A. Streicher, "Spectra-cular" Measurements, Optik & Photonik 12 (4) (2017) 38–40.
[26] https://www.micro-epsilon.com/2D_3D/boreCONTROL/; [accessed 15 February 2018].
[27] P. J. Besl, N. D. McKay, et al., A method for registration of 3-D shapes, IEEE Transactions on pattern analysis and machine intelligence 14 (2) (1992) 239–256.
[28] D. Haehnel, S. Thrun, W. Burgard, An extension of the ICP algorithm for modeling nonrigid objects with mobile robots, in: IJCAI, Vol. 3, 2003, pp. 915–920.